J Pharmacol Sci **115**, 15 – 26 (2011)

Journal of Pharmacological Sciences

Full Paper

Bepridil Facilitates Early Termination of Spiral-Wave Reentry in Two-Dimensional Cardiac Muscle Through an Increase of Intercellular Electrical Coupling

Hiroki Takanari[1], Haruo Honjo[1,*], Yoshio Takemoto[1], Tomoyuki Suzuki[1], Sara Kato[1], Masahide Harada[1], Yusuke Okuno[1], Takashi Ashihara[2], Tobias Opthof[3,4], Ichiro Sakuma[5], Kaichiro Kamiya[1], and Itsuo Kodama[1]

[1]*Department of Cardiovascular Research, Research Institute of Environmental Medicine, Nagoya University, Nagoya 464-8601, Japan*
[2]*Department of Cardiovascular and Respiratory Medicine, Shiga University of Medical Science, Otsu 520-2121, Japan*
[3]*Experimental Cardiology Group, Center for Heart Failure Research, Academic Medical Center, Amsterdam 1105AZ, The Netherlands*
[4]*Department of Medical Physiology, University of Utrecht, Utrecht 3584CM, The Netherlands*
[5]*Graduate School of Engineering, The University of Tokyo, Tokyo 113-8656, Japan*

Received September 10, 2010; Accepted October 29, 2010

Abstract. Bepridil is effective for conversion of atrial fibrillation to sinus rhythm and in the treatment of drug-refractory ventricular tachyarrhythmias. We investigated the effects of bepridil on electrophysiological properties and spiral-wave (SW) reentry in a 2-dimensional ventricular muscle layer of isolated rabbit hearts by optical mapping. Ventricular tachycardia (VT) induced in the presence of bepridil (1 μM) terminated earlier than in the control. Bepridil increased action potential duration (APD) by 5% – 8% under constant pacing and significantly increased the space constant. There was a linear relationship between the wavefront curvature (κ) and local conduction velocity: $LCV = LCV_0 - D \cdot \kappa$ (D, diffusion coefficient; LCV_0, LCV at $\kappa = 0$). Bepridil significantly increased D and LCV_0. The regression lines with and without bepridil crossed at $\kappa = 20 – 40$ cm^{-1}, resulting in a paradoxical decrease of LCV at $\kappa > 40$ cm^{-1}. Dye transfer assay in cultured rat cardiomyocytes confirmed that bepridil increased intercellular coupling. SW reentry in the presence of bepridil was characterized by decremental conduction near the rotation center, prominent drift, and self-termination by collision with boundaries. These results indicate that bepridil causes an increase of intercellular coupling and a moderate APD prolongation, and this combination compromises wavefront propagation near the rotation center of SW reentry, leading to its drift and early termination.
[Supplementary Figures: available only at http://dx.doi.org/10.1254/jphs.10233FP]

Keywords: bepridil, spiral-wave reentry, intercellular coupling, optical mapping, ventricular tachycardia

Introduction

Bepridil has both antianginal and antiarrhythmic effects (1). Clinical evidence suggests that bepridil is effective in the treatment of ventricular tachyarrhythmias refractory to other antiarrhythmic drugs (2, 3). Recently, bepridil was also shown to be effective in conversion of persistent atrial fibrillation and subsequent maintenance of sinus rhythm (4, 5). However, there remain concerns about the drug-induced polymorphic ventricular tachycardia (VT), known as torsades de pointes (TdP) in association with excessive QT prolongation, especially at high doses, in patients with structural heart disease (5). The pharmacological profile of bepridil is complex, and

*Corresponding author. honjo@riem.nagoya-u.ac.jp
Published online in J-STAGE on December 9, 2010 (in advance)
doi: 10.1254/jphs.10233FP

a plethora of molecular targets of drug action have been reported. As to the cell membrane events, bepridil inhibits its Ca^{2+} (L-type and T-type), K^+, Na^+ channels, and the Na^+/Ca^{2+} exchanger (6 – 9). The affected K^+ channels include ultrarapid, rapid, and slow activation components of the delayed rectifier K^+ current (I_{Kur}, I_{Kr}, I_{Ks}) (10, 11); the transient outward current (I_{to}) (12); and various types of ligand-gated K^+ currents including muscarinic acetylcholine-activated K^+ current ($I_{K,ACh}$), Na^+-activated K^+ current ($I_{K,Na}$), and sarcolemmal ATP-sensitive K^+ current ($I_{K,ATP}$) (13 – 15). However, bepridil has been reported to open mitochondrial ATP-sensitive K^+ channels (15). The inhibitory action against K^+ and Ca^{2+} channels are, by and large, more potent than that against Na^+ channels (6, 7). As to the intracellular events, bepridil inhibits calmodulin-dependent processes, for example, myosin light-chain kinase phosphorylation required for vascular smooth muscle contraction (1, 16). The Ca^{2+} affinity of cardiac troponin C is increased by bepridil (17). Despite extensive experimental studies reported so far, much remains to be clarified on the exact mechanisms of the unique and potent antiarrhythmic action.

It is generally believed that regardless of the initiating event, spiral- or vortex-type reentrant activity rotating around a functional obstacle (rotor) is the major organization center of VT / ventricular fibrillation (VF) and atrial fibrillation (18, 19). Bepridil's potent antiarrhythmic activity could be the result of a specific modification of spiral-wave (SW) reentry in cardiac muscle. To address this issue, we investigated the effects of bepridil on the electrophysiological properties of the 2-dimensional subepicardial ventricular myocardium of rabbit hearts.

We have found that bepridil increases intercellular electrical coupling of cardiac muscle, and compromises wavefront propagation at regions of high curvature as in the rotation center of SW reentry. This favors early self-termination of the reentry.

Materials and Methods

Optical mapping experiments

The protocol was approved by the Institutional Animal Care and Use Committee at Nagoya University. The experimental model and procedures of optical mapping are essentially the same as reported previously (20 – 22). Briefly, isolated rabbit hearts (n = 27) were perfused on a Langendorff apparatus with modified Krebs-Ringer solution (equilibrated with 95% O_2 – 5% CO_2) at 37°C. Complete atrioventricular block was produced by destruction of the His bundle. A 2-dimensional epicardial layer of ventricular myocardium (approximately 1-mm-thick) was prepared by cryoprocedure of the left ventricular (LV) endomyocardium and was stained with a voltage-sensitive dye, di-4-ANEPPS. 2,3-Butandione monoxime (BDM) was applied to minimize motion artifacts. Bipolar electrograms were recorded through widely spaced electrodes to monitor ventricular activation.

The hearts were illuminated by bluish-green light emitting diodes (LEDs) and the fluorescence was recorded with a high-speed digital video camera to acquire 10-bit gray scale images (256 × 256 pixels) at a sampling rate of 1,000 frames/s. The image covered the anterolateral surface (30 × 30 mm) of the LV. To reveal the action potential signal, the background fluorescence was subtracted and low-pass filtering was applied. Spatial resolution after the filtering was 0.1 mm. Isochrone maps of 1 – 4 ms intervals were generated from the filtered image. From normalized action potential signals, time points at 10% depolarization and 90% repolarization were identified, and their interval was defined as action potential duration (APD). Wave propagation patterns during VT were analyzed by the phase-mapping method (23).

Measurement of conduction velocity (CV) and APD

Global CV and APD were measured during longitudinal propagation of linear excitation waves. At the beginning of each experiment, the direction of the fastest propagation in the center of the LV free wall was determined by stimulation with a monopolar electrode (diameter, 0.1 mm). Then, the central electrode was removed and a monopolar line electrode made of a fine Ag wire (diameter, 0.1 mm) was placed near the LV base to produce longitudinal propagation of the flat excitation front. Global CV was calculated from the slope of a linear least square fit of the activation time plotted against the distance.

Induction of VT

VTs (lasting ≥3 beats) were induced by modified cross-field stimulation. Nineteen basic (S1) stimuli [basic cycle length (BCL), 400 ms] were applied to the LV apex through a pair of contiguous bipolar electrodes, and a 20-ms monophasic pulse (20 V) was delivered through a pair of paddle electrodes (diameter, 7 mm) placed on the lateral surface of both ventricles for the DC stimulation (DS2) to induce an electrical field in a direction perpendicular to the S1 excitation. The S1-DS2 coupling interval was shortened progressively at 10-ms steps to cover the whole vulnerable window. When VTs sustained ≥60 s, they were terminated by application of DC shocks (20 ms, monophasic pulse at 60 – 80 V).

Estimation of intercellular electrical coupling

Intercellular electrical coupling was estimated by two protocols: measurement of the space constant (λ) and the

diffusion coefficient (D). In these experiments, magnified fluorescence images (each 256 × 256 pixels) covering a square of 5 × 5 mm were obtained through a photographic lens with a longer focal distance (Micro-Nikkor 105 mm, f/2.8D; Nikon, Tokyo) at a sampling rate of 1,000 frames/s.

The space constant (λ) was measured by the previously described method (24, 25). In brief, a single cathodal subthreshold stimulus (20 ms in duration, approximately 0.8 times threshold) was delivered during electrical diastole after regular (BCL, 400 ms) suprathreshold stimuli (2.0 ms in duration, approximately 1.2 times the threshold intensity) through a teflon-coated platinum wire electrode (diameter, 0.1 mm) placed at the center of the anterior LV free wall. To induce subthreshold membrane potential responses, myocardial excitability was reduced by an elevation of the extracellular K^+ concentration from 4 to 8 mM. Membrane responses to subthreshold stimuli were estimated at the maximum change in fluorescence intensity relative to the resting level and normalized with respect to the amplitude of baseline action potential signals at each recording site.

The relationship between the wavefront curvature (κ) and local CV (LCV) was analyzed for the elliptical wavefront propagating from a single stimulation point to estimate the diffusion coefficient (D). According to the model analysis by Zykov and Morozova in a continuous 2-dimensional excitable medium, the relationship between LCV and κ is expressed by the following equation (26):

$$LCV = LCV_0 - D \cdot \kappa \qquad [1]$$

, where LCV_0 is LCV at a flat wavefront (i.e., $\kappa = 0$). D is determined by the passive properties of the excitable medium (proportional to the inverse of the intercellular resistance) (26). In these experiments, pulses (2 ms in duration, 1.2 times the threshold intensity) were applied to the center of the anterior LV wall via a monopolar teflon-coated platinum wire electrode (0.1 mm in diameter). The isochrone of the activation wavefront with variable distance from the stimulation site (0.2 – 3 mm in the longitudinal direction) was fitted by an ellipse, and long (a) and short (b) semiaxes of the respective ellipse (in the longitudinal and transverse directions, respectively) were measured. The local curvature at the longitudinal apex was calculated from the two semiaxes (a/b^2) (27). The propagation velocity of the wavefront at the site of measurement (longitudinal apex) was estimated from the partial derivatives of the CV vector field, according to the methods originally described by Bayly et al. (28).

Dye transfer assay

To estimate the intercellular communication through gap junctions, we performed a dye transfer assay on cultured cardiomyocytes obtained from 1-day-old rat neonates as described previously (29). Lucifer yellow CH (LY, 2 mM) was micro-injected into a single cardiomyocyte of each confluent monolayer, and at 5 min after the dye injection, cardiomyocytes were fixed by 2% paraformaldehyde. Confocal images were obtained by laser scanning microscopy (LSM-510; Carl Zeiss, Oberkochen, Germany) and the number of LY-stained cells was counted.

Statistical analyses

Data were expressed as means ± standard error of the mean (S.E.M.). Statistical comparisons were performed by ANOVA with the Bonferroni post hoc test, Student's t-test, or covariance analysis when appropriate. Differences were considered significant when $P < 0.05$.

Results

Basic electrophysiological properties

Global CV and APD were measured during longitudinal propagation of linear excitation waves at BCL 150 – 400 ms (Fig. 1A). Bepridil caused variant changes of global CV (Fig. 1B): global CV increased significantly with 1 μM bepridil at BCL 150 – 400 ms (by 7% – 10%). With 5 μM bepridil, in contrast, global CV significantly decreased compared to the control at BCL 150 ms, but significantly increased at BCL 200 and 400 ms. Figure 1C illustrates a representative example of changes of APD at BCL 400 ms. APD values in the mapping area are displayed as color gradients (left), and optical action potential signals obtained from 16 sites (covering an 18 × 18 mm square) are superimposed (right). Figure 1D summarizes the effects of bepridil on APD. Bepridil at 1 μM significantly increased APD at BCL 150 – 400 ms (by 5% – 8%), and a higher concentration of bepridil (5 μM) caused a greater increase of APD. The APD prolongation by bepridil showed no substantial frequency-dependency within the range of BCLs tested. Spatial dispersion of APD among the 16 recording sites was unchanged by 1 μM bepridil compared to the control, whereas it increased significantly at 5 μM (Fig. 1E).

VTs induced by DC stimulation

VTs were induced by modified cross-field stimulation in 12 hearts, and the incidence of sustained-VTs (lasting ≥60 s) as a percentage of all VTs was compared before and after drug application (Fig. 2). With 1 μM bepridil, sustained-VTs occurred in all 6 hearts in the controls and in 3 of the 6 hearts after drug application. The percentage of sustained-VTs / heart decreased significantly from 34 ± 3% to 6 ± 3% ($P < 0.01$). With 5 μM bepridil, sus-

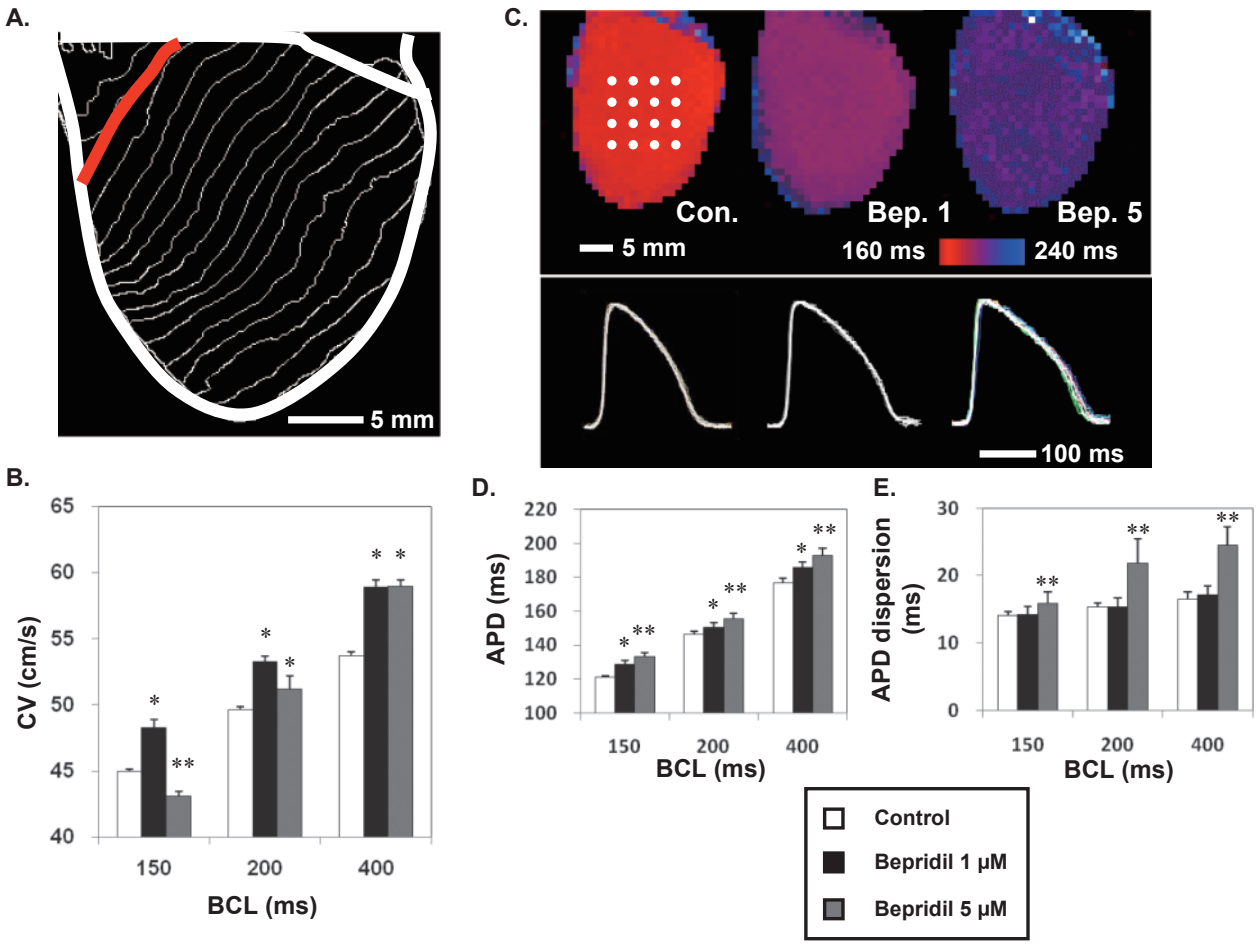

Fig. 1. Effects of bepridil on APD and global CV. A: Isochrone activation map (5-ms intervals) during longitudinal propagation of linear excitation waves. Constant electrical stimuli (BCL, 400 ms) were applied through a wire electrode placed near the base of the LV free wall (red line). B: Global CV at BCLs of 150, 200, and 400 ms. Data were obtained before (control) and after application of bepridil at 1 and 5 μM bepridil (n = 5). C: APD color gradient maps in the LV free wall (top) and superimposed action potential signals (bottom) recorded from 16 sites (white dots in top panel) covering an 18 × 18 mm area under constant stimulation (BCL, 400 ms) before (control) and after application of bepridil at 1 and 5 μM. D, E: APD (D) and its spatial dispersion (E) defined by the difference between the maximum and minimum measured at 16 sites, at BCLs of 150, 200, and 400 ms. Data were obtained before (control) and after application of bepridil at 1 and 5 μM bepridil (n = 5). *$P < 0.05$, **$P < 0.01$ vs. control.

tained-VTs occurred in all 6 hearts in controls and after drug application. The percentage of sustained-VTs / heart tended to decrease from 33 ± 4% to 23 ± 3%, but remained insignificant. Similar concentration-dependent effects of bepridil on the VT sustainability were observed in experiments in the absence of BDM (Supplementary Fig. 1: available in the online version only).

These observations show that bepridil has different effects on APD and global CV of ventricular myocardium at 1 and 5 μM. Persistence of VT is prevented by bepridil only at the lower concentration. Therefore, the following part of this study focuses on the antiarrhythmic mechanism of 1 μM bepridil.

Intercellular coupling

It is intriguing that 1 μM bepridil increases CV because the acute effect of bepridil is considered to be suppression of excitability by Na^+ channel–blocking action (1, 6, 7). Therefore, we hypothesized that the bepridil-induced increase of CV is the result of a modification of intercellular coupling.

To address this hypothesis, we first measured λ in the absence and presence of 1 μM bepridil. Application of subthreshold cathodal monopolar stimuli resulted in electrotonic membrane depolarizations localized in the vicinity of the stimulus electrode, whereas the suprathreshold stimuli induced propagating action potentials (Fig. 3A). The amplitude of subthreshold depolarization decreased almost exponentially with increasing distance

from the stimulation site (Fig. 3B). Bepridil increased λ along and across the fiber orientation (λ_L, 1.29 ± 0.05 vs. 1.08 ± 0.06 mm; λ_T, 1.08 ± 0.06 vs. 0.84 ± 0.04 mm, n = 5, $P < 0.01$; Fig. 3C).

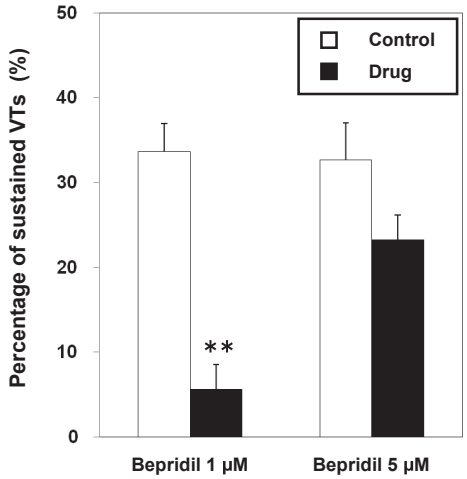

Fig. 2. Effects of bepridil on the incidence of sustained-VTs (≥60 s) induced by modified cross-field stimulation. The incidence was assessed on the basis of VT episodes per heart. Data were obtained before (control) and after application of 1 and 5 μM bepridil (n = 6). **$P < 0.01$ vs. control.

Next, we investigated the effects of 1 μM bepridil on the relationship between κ and LCV during centrifugal propagation to estimate D. Figure 4A shows isochrones of activation in the vicinity of the stimulation electrode. The wavefronts close to the stimulation point (0.2 – 3 mm in the longitudinal direction) were fitted by ellipses, and κ at the longitudinal apex was calculated from their long and short semiaxes. Representative data are shown in Fig. 4B. There was a linear relationship between the two parameters; the higher the κ, the smaller the LCV. The slope of the regression line, which represents D, was significantly greater in the presence of bepridil (0.62 cm^2/s) than in the control (0.42 cm^2/s, $P < 0.01$, covariance analysis), giving rise to crossover of the two regression lines. Consequently, LCV after bepridil was larger than in the control at $\kappa < 20$ cm^{-1}, whereas it was smaller than in the control at $\kappa > 40$ cm^{-1}. LCV_0 was 55.8 cm/s in the control and 59.8 cm/s after bepridil in this experiment. The difference between the regression lines before and after bepridil reached the same level of significance in the other 4 experiments (not shown). Figure 4C summarizes the data obtained from all 5 hearts. D (slope of regression lines) and LCV_0 were increased significantly after bepridil (D, 0.56 ± 0.02 vs. 0.39 ± 0.01 cm^2/s, $P <$

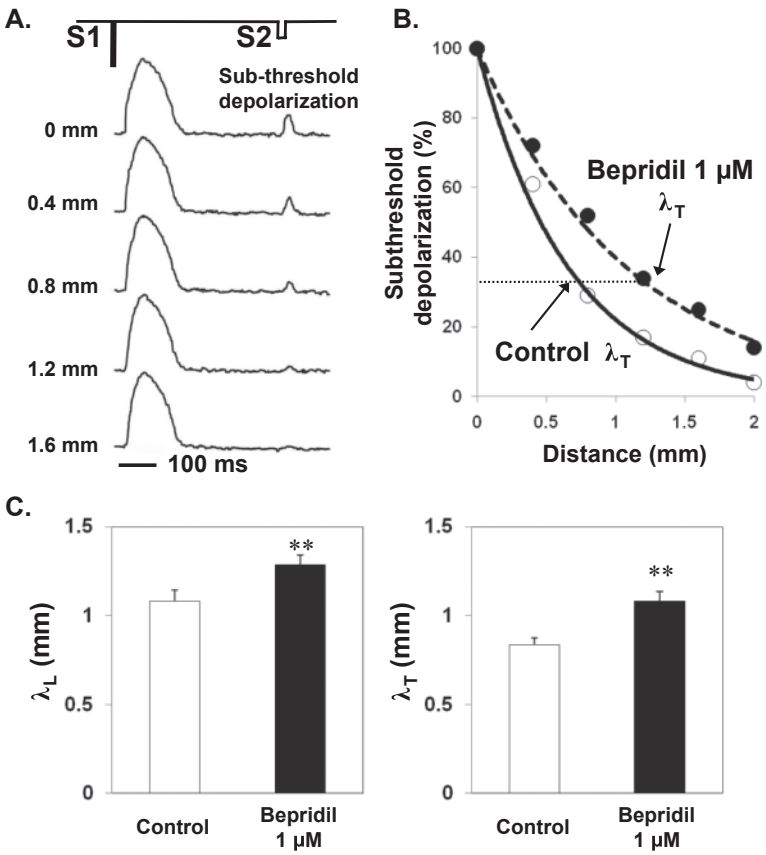

Fig. 3. Space constant (λ) assessed by decline of electrotonic membrane depolarization. A: Typical example of optical recording of membrane depolarization in response to supra (S1) and subthreshold (S2) stimuli. The records were obtained for sites 0 – 1.6 mm from the stimulation electrode in the transverse direction of propagation. B: Distance vs. decay of subthreshold depolarization in the transverse direction before (control) and after application of 1 μM bepridil. λ was calculated from the exponential decay constant. C: λ values in the longitudinal and transverse directions (λ_L and λ_T, respectively) before (control) and after bepridil (n = 5). **$P < 0.01$.

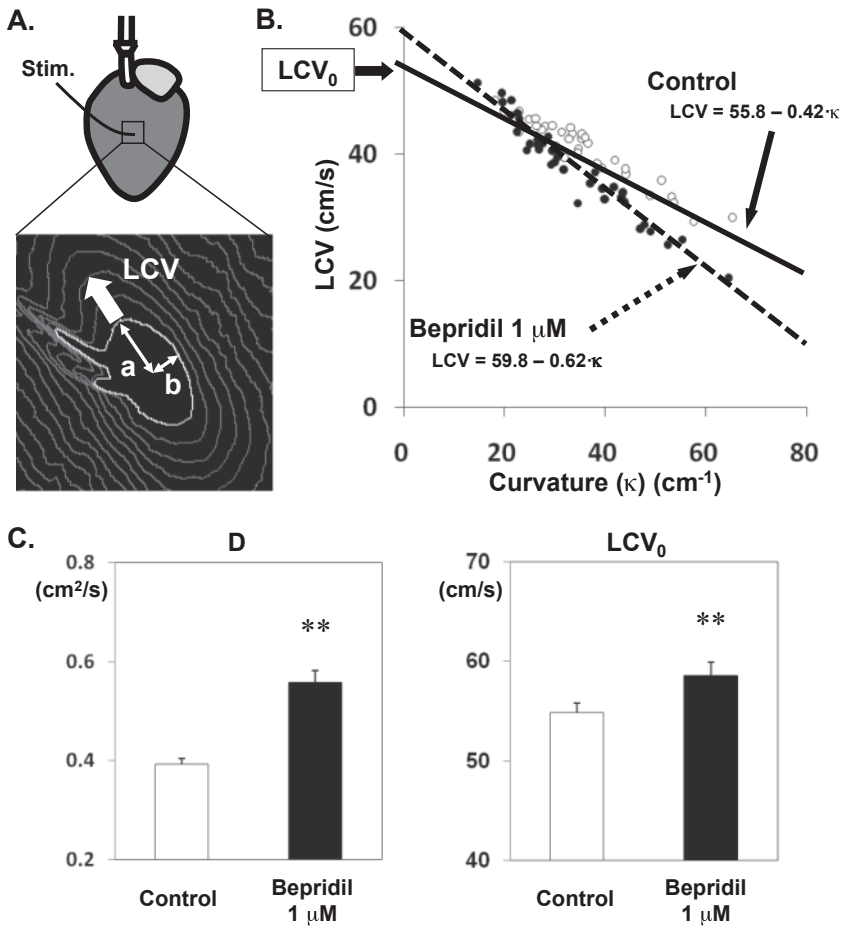

Fig. 4. Effects of bepridil on the relationship between wavefront curvature (κ) and local conduction velocity (LCV). A: κ and LCV values in the longitudinal direction were measured form isochrones (1-ms intervals) in a small area (5 × 5 mm) during centrifugal propagation under constant stimulation (BCL, 400 ms). The wavefronts close to the stimulation site were fitted by ellipses with long (a) and short (b) semiaxes, and κ at the longitudinal apex of the ellipse was calculated from a/b^2. LCV at the respective site was estimated from the vector field. Protrusions of isochrones are artifacts produced by the stimulation electrode and its shadow. B: Representative results obtained from one heart; the measurements were made before and after application of 1 μM bepridil, and each LCV was plotted against the respective κ. There was a linear relationship between the two parameters: LCV = 55.8 − 0.42·κ for the control (r^2 = 0.915) and LCV = 59.8 − 0.62·κ for bepridil (r^2 = 0.944). LCV_0 (LCV at κ = 0) was 55.8 cm/s for the control and 59.8 cm/s for bepridil. The difference between the two regression lines was significant ($P < 0.01$, covariance analysis). C: Summarized data of the slope of regression lines, which represents D, and LCV_0 in the control and after bepridil (n = 5). **$P < 0.01$.

0.01; LCV_0, 58.6 ± 1.3 vs. 54.9 ± 0.9 cm/s, $P < 0.01$).

We also examined the effect of bepridil on the intercellular communication in monolayers of cultured neonatal rat cardiomyocytes by dye-transfer assay using Lucifer yellow (Fig. 5). The number of dye-coupled cells in the cultures treated with 1 μM bepridil was significantly larger than in the control by 40.7%.

Dynamics of SW reentry

Optical images of excitation during VTs were analyzed in 5 hearts exhibiting visible SW reentry before and after application of 1 μM bepridil. Figure 6, A and B, shows a representative experiment. Under control conditions (30 s after VT initiation), a counterclockwise rotor circulating around a line of functional block (FBL, approximately 4 mm in length) can be seen at CL of 132 – 135 ms (Fig. 6A, left). The circuit was stable for >60 s. The distant bipolar electrogram (ECG) showed monomorphic excitations. In the phase map, a phase singularity (PS) moved back and forth along the FBL. The trajectory of the PS during three consecutive excitations was illustrated on the phase map (Fig. 6A, right).

Figure 6B shows activation patterns during a short polymorphic VT (lasting 5 s) after application of 1 μM bepridil (the last three beats prior to self-termination). SWs changed their circuits in a beat-to-beat manner with CLs varying from 141 to 162 ms. In beat *i*, a rotor circulated counterclockwise around an "I"-shaped FBL (6 mm). In beat *ii*, the rotation was shifted to the right and maintained around a longer "Y"-shaped FBL. In beat *iii*, the right arm of the "Y"-shaped FBL was extended upward. Consequently, the rotation center drifted upward and finally collided with the atrioventricular groove. The PS trajectory during these beats was illustrated in the phase map. A PS initially moved from the center toward the right lower region, then back toward the upper region, and finally collided with the atrioventricular groove.

Qualitatively similar changes of SW reentry leading to early VT termination were observed in the other 4 hearts after application of 1 μM bepridil. The transformation was characterized by long and curved FBLs and prominent drift of the reentry circuit (Fig. 6C). The average length of the PS trajectory per unit of time (1 s) increased significantly from 8.8 ± 2.1 cm in the control to 12.5 ± 3.3 cm after bepridil (Fig. 6D, left). The average VT-CL increased from 127.4 ± 11.2 ms in the control to

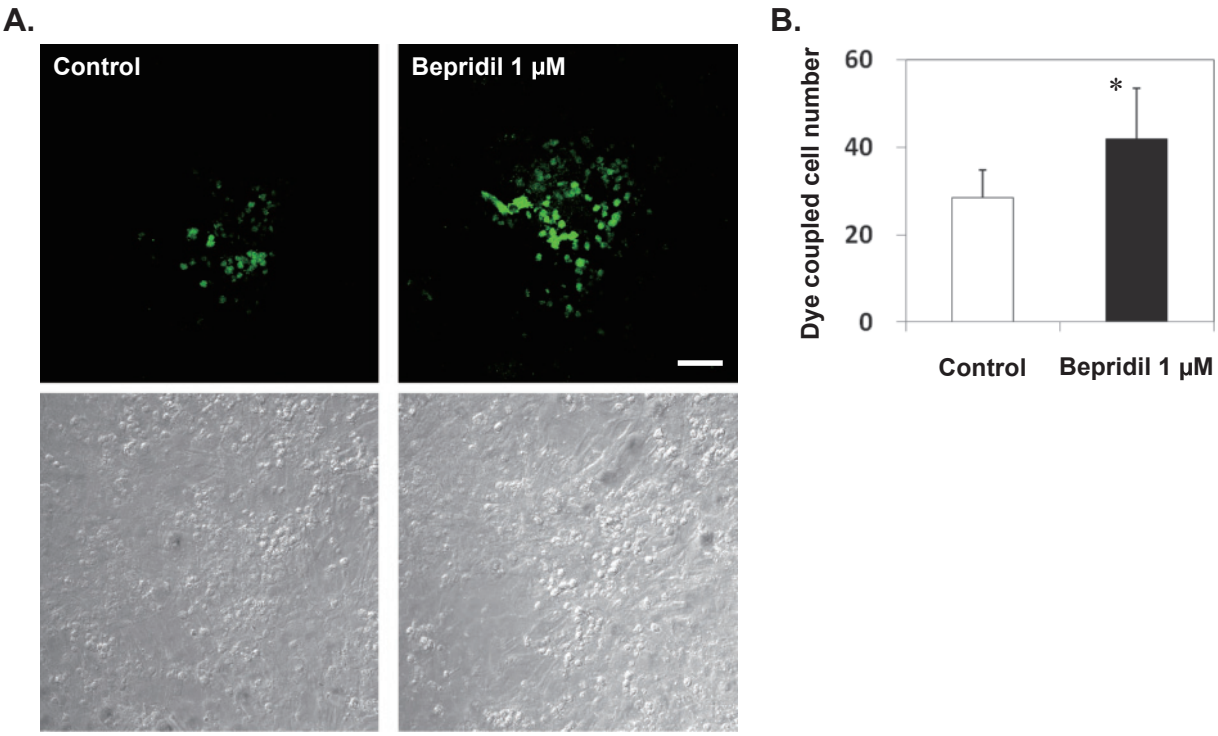

Fig. 5. Dye-transfer assay using a gap junction–permeable fluorescent dye. A: Representative confocal fluorescent microscopic images (top) and corresponding phase contrast images (bottom) of cultured neonatal rat cardiomyocytes after micro-injection of Lucifer yellow. Left: Untreated culture of cardiomyocytes (control). Right: Cardiomyocytes treated with 1 μM bepridil for 30 min. Scale bar, 100 μm. B: The number of dye-coupled cells in the culture treated with bepridil was significantly larger than in the control (n = 14). *$P < 0.05$.

160.5 ± 13.6 ms after bepridil (Fig. 6D, right). The average number of PSs (per 1 s) observed in the recording area was, however, comparable before and after bepridil (1.10 ± 0.23 vs. 1.16 ± 0.17, NS).

Figure 7 shows characteristic features of action potential signals in association with a drift of the reentry circuit in the presence of bepridil. Isochrone activation maps are from three consecutive beats in another episode of a short (17 s) polymorphic VT (in the same heart as presented in Fig. 6). In beat *i*, a rotor circulated counterclockwise in the center of the LV anterior wall (Fig. 7A). Action potential signals *a-b-c-d* (outer limb) and *a-e-f-g* (inner limb) showed similar propagation toward the apex, constructing the left arm of the counterclockwise circuit (Fig. 7B). In beat *ii*, the wavefront in the outer limb (*a-b-c-d*) was preserved, but that in the inner limb (*a-e-f-g*) showed decremental conduction, giving rise to the formation of an "L"-shaped FBL. In beat *iii*, the activation wavefront from *d* proceeded upward through *g*, *f*, and *e*, constructing the right arm of the circuit around a "Y"-shaped FBL. Consequently, the circuit was shifted toward the left during the three beats.

Similar sequences of events were observed in the other 4 hearts in the presence of bepridil, suggesting that decremental conduction close to the rotation center may play a pivotal role in the bepridil-induced drift of SWs.

Discussion

Key observations on the effect of 1 μM bepridil in this study are as follows: 1) Bepridil causes a moderate prolongation of APD and a moderate increase of global CV. 2) It decreases the persistence of VTs. 3) It increases the space constant. 4) It increases the diffusion coefficient estimated from the slope between the wavefront curvature and LCV. 5) SW reentry in the presence of bepridil is characterized by decremental conduction near the rotation center, giving rise to a prominent drift of the circuit, and self-termination.

Action potential and conduction properties

In this study, we first examined the effects of bepridil on action potential configuration and global CV. Bepridil at 1 μM caused a moderate and frequency-independent prolongation of APD in association with significant increases of global CV. At a higher concentration (5 μM)

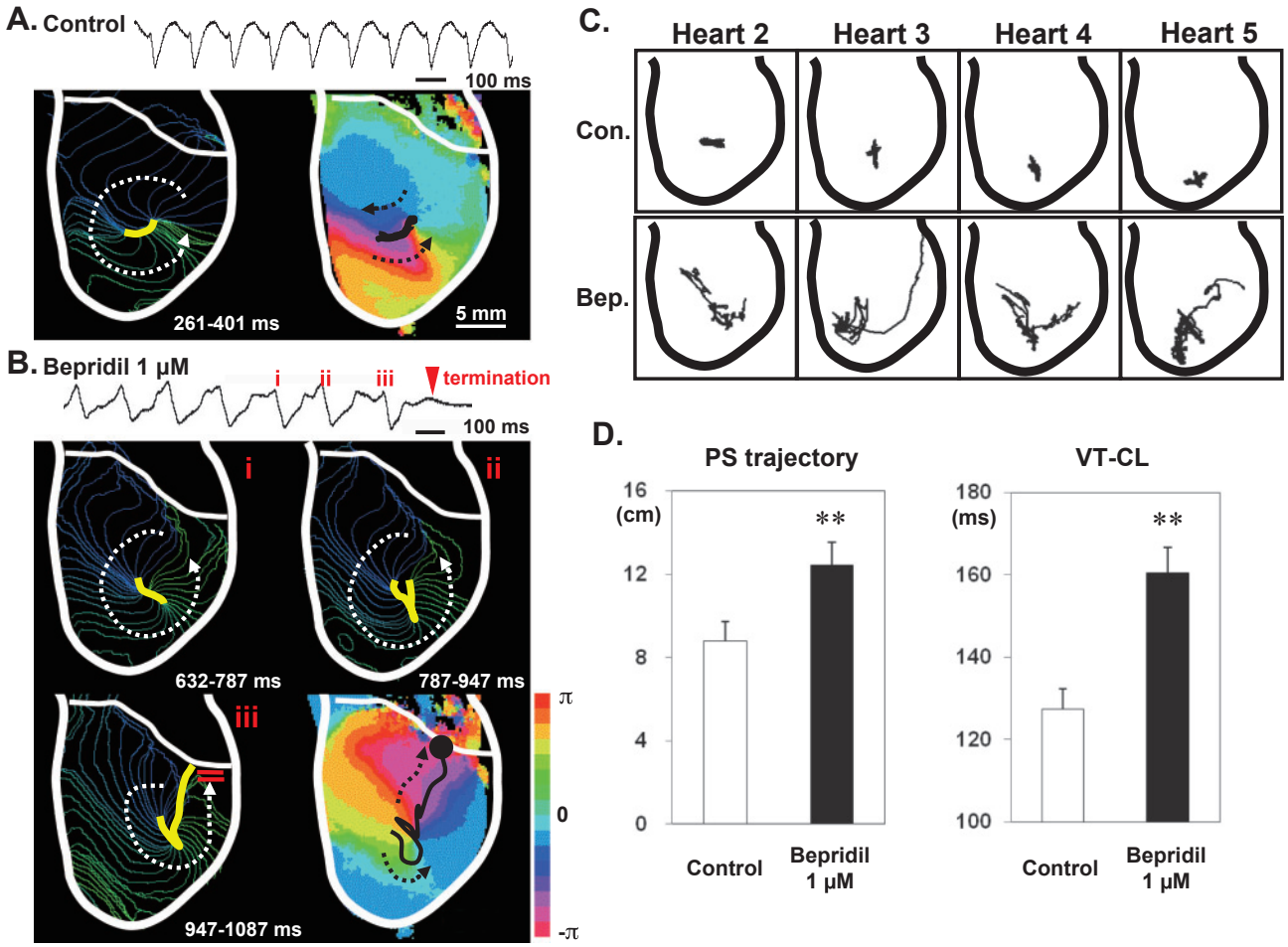

Fig. 6. SW excitations during VT before (control) and after application of 1 μM bepridil. A: Sustained monomorphic VT under the control condition. Top: bipolar electrogram. Bottom: isochronal activation map (5-ms intervals with varying colors from blue to green, left) and phase map (right) with PS trajectory (black line) during three consecutive beats. A stable SW circulated counterclockwise around a FBL (yellow) with CLs of 132 – 135 ms. B: Non-sustained polymorphic VT in the presence of 1 μM bepridil. Top: bipolar electrogram. Bottom: isochronal activation maps during the last three beats (*i*, *ii*, *iii*) prior to VT termination and phase map with PS trajectory (black line). An unstable SW circulated counterclockwise around an FBL of various configurations with CLs of 141 – 162 ms. A PS drifted tremendously and finally collided with the atrioventricular groove. C: PS trajectory during VTs before and after 1 μM bepridil in 4 hearts. D: Average length of PS trajectory per unit of time (1 s) and average VT-CL in the control and after bepridil (n = 5). $^{**}P < 0.01$.

of bepridil, the APD prolongation was further enhanced, but the effect on CV was frequency-dependent; CV still increased at BCL 200 – 400 ms, but decreased at BCL 150 ms. These bepridil-induced alterations in the steady-state electrophysiological properties of ventricular muscle can be ascribed partly to its multi-channel blocking actions.

It has been reported that bepridil at therapeutic concentrations prolongs APD in ventricular muscle of guinea pig, dog, and rabbit (30 – 32). The APD prolongation in guinea pig, unlike most of other class-III antiarrhythmic drugs, shows minimal "reverse use-dependence" (28). Similar frequency-independent APD prolongation has been demonstrated in humans by recording monophasic action potentials (33). Our observation is concordant with these previous reports. The bepridil-induced frequency-independent APD prolongation is most likely attributable to the inhibition of both I_{Kr} and I_{Ks} because the contribution of I_{Kr} to ventricular repolarization is larger at slower rates, whereas that of I_{Ks} is larger at faster rates.

The inhibition of CV by 5 μM bepridil, which was restricted to the shortest BCL (150 ms), can be readily understood by use-dependent block of Na^+ channels (1, 6, 7). The increase of CV by bepridil, however, cannot be explained by changes in membrane currents.

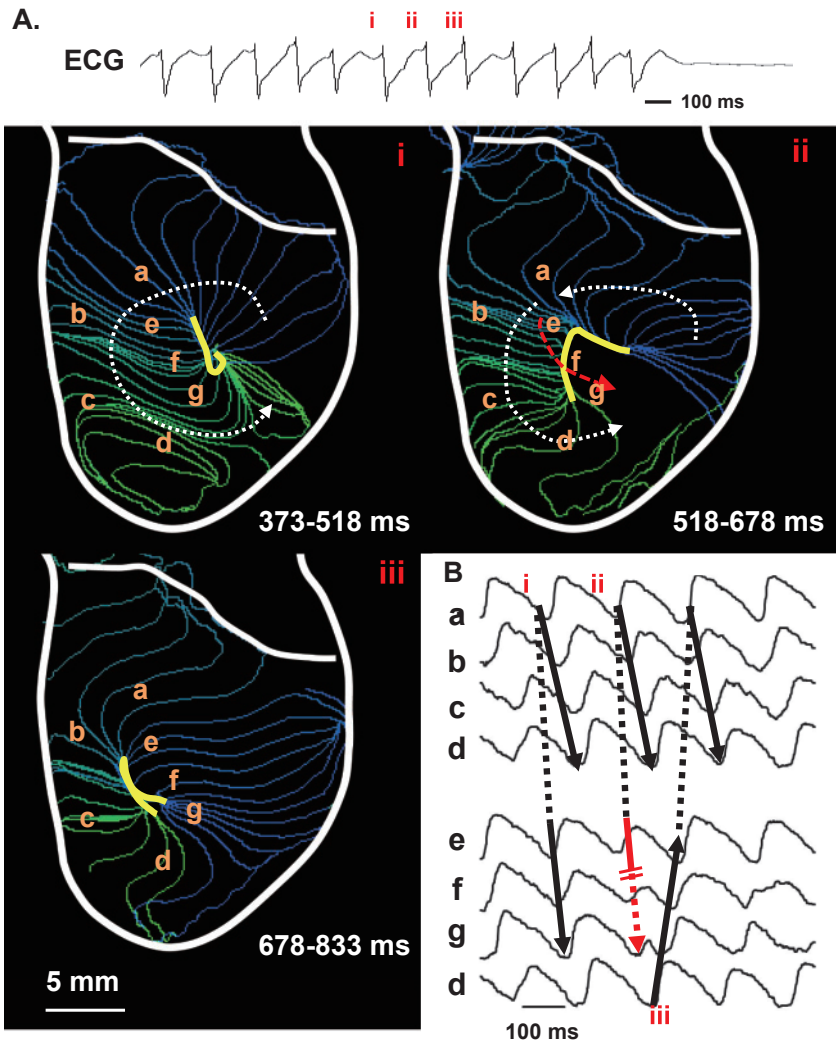

Fig. 7. Characteristic features of action potential signals in association with the drift of SW reentry in the presence of 1 μM bepridil. A: Isochronal activation maps (5-ms intervals) of three consecutive beats during a short polymorphic VT (*i*, *ii*, and *iii* in ECG, top). The circuit of counterclockwise rotation drifted from right to left in association with beat-to-beat alterations of FBL (yellow line) configuration. B: Action potential signals recorded from 7 sites in the circuit (*a* to *g*). The signals showed decremental conduction close to the rotation center (*a-e-f-g*, red dotted arrow in A, beat *ii*), and subsequent reversal of propagation sequence in this region (beat *iii*).

Effects of bepridil on the intercellular electrical coupling

According to cable theory, CV is inversely proportional to the square root of tissue resistivity, which is composed of intracellular and extracellular resistances (R_i and R_o, respectively). The value of λ estimated from the spatial decay of electrotonic depolarization in response to subthreshold stimuli is proportional to the square root of membrane resistance (R_m) / tissue resistance ($R_o + R_i$) (26). Bepridil (1 μM) significantly increased λ both along and across the fiber orientation (by 21% – 34%). In order to estimate the contribution of bepridil-induced changes in R_m to the increase of λ, we carried out patch clamp experiments in single rabbit ventricular myocytes: R_m increases by 16.4 ± 1.6% in the presence of 1 μM bepridil (n = 5, unpublished data), and this would cause an increase of λ by only approximately 11%. Therefore, bepridil must cause an additional decrease of R_i, provided that R_o is unaffected.

CV in cardiac muscle is affected by the wavefront curvature. When the excitation wavefront is convex, the CV is lower than in the case of a flat wavefront because the local excitatory current supplied by the upstream cells distributes over a larger area downstream (source-sink mismatch). In 2-dimensional isotropic excitable media, this curvature effect is expressed by Eq [1] (26). Our high-resolution optical mapping enabled analysis of centrifugal propagation in the vicinity of a stimulation site and revealed that there is a linear relationship with a negative slope between the κ and the LCV as expected from Eq [1].

Although Eq [1] assumes that the excitable medium is isotropic, the real cardiac tissue is anisotropic with different CV values in the longitudinal and transverse directions. As a consequence, initiation of electrical activity in cardiac tissue by point stimulation results in a wavefront having an elliptical shape as shown in Fig. 4, and the relationship in the anisotropic cardiac tissue can be

theoretically described as follows (34, 35):

$$LCV_L = LCV_{L0} - D_T \cdot \kappa_L \quad [2]$$

$$LCV_T = LCV_{T0} - D_L \cdot \kappa_T \quad [3]$$

, where subscripts L and T refer to longitudinal and transverse directions, respectively. Our data plotting LCV against κ in the longitudinal direction is, therefore, formulated by Eq [2], and the D value represents D_T.

The D value (0.39 cm^2/s) obtained from the slope of the regression line under control conditions was comparable to those estimated from single point measurement of the elliptical activation wavefront (36) and in a mathematical model analysis of curved wavefronts through a narrow isthmus (27, 35). To the best of our knowledge, our data are the first direct estimation of D by plotting LCV against κ in 2-dimensional real ventricular muscle. The D value measured in the presence of 1 μM bepridil was significantly larger (0.56 cm^2/s) compared to the control.

Taken together, these results suggest that bepridil enhances intercellular electrical coupling of ventricular muscle. Our observation in the dye-transfer experiments in cultured cardiomyocytes provides additional evidence for bepridil-induced increase of intercellular communication through gap junctions.

Bepridil has been shown to inhibit a variety of intracellular calmodulin-dependent processes (1, 16). There are considerable evidences indicating that calmodulin is involved in the Ca^{2+}-dependent regulation of gap junction conductance (37, 38). Calmodulin binding motif in the juxtamembrane region of the intracellular loop of Cx43 has recently been identified by Zhou et al. (39). Accordingly, it seems reasonable to speculate that bepridil would increase Cx43 gap junction conductance through prevention of Ca^{2+}-calmodulin-dependent modification of the channel conformation. Further experimental studies will be required to substantiate this speculation.

Destabilization and early termination of SW reentry

SW dynamics during VTs induced in the presence of 1 μM bepridil were characterized by a longer CL, a prolongation and deformation of FBLs, and a prominent drift of the reentry circuits leading to self-termination by collision with the anatomical boundaries. The VT was transformed from monomorphic to polymorphic and from sustained to non-sustained. We demonstrated previously that nifekalant, a selective I_{Kr} blocker, caused destabilization and early termination of SW reentry in association with marked prolongation and deformation of FBLs (20). This suggests that the bepridil-induced modification of SW reentry is caused, partly, by the APD prolongation through blockade of I_{Kr} and I_{Ks}.

However, there are also substantial differences between the effects of the two drugs. In the presence of nifekalant, the wavefront frequently encountered its own tail, causing a transient wave break-up (20). Bepridil, in contrast, destabilized the rotation center of reentry without enhancement of wavefront-tail interactions. An increase in the intercellular electrical coupling by bepridil is considered to be involved in this unique modification. From our analysis (Fig. 4), CV of the convex wavefront at $\kappa > 40$ cm^{-1} is suppressed by bepridil. The conceptual critical wavefront curvature (κ_c) to block the wave propagation (LCV_0/D) (26) would be decreased from 139.7 cm^{-1} in the control to 105.2 cm^{-1} after bepridil on average. In other words, reentrant circuits with extreme convexity will be aborted in the presence of 1 μM bepridil.

Another mechanism to be considered for bepridil-induced destabilization is anchoring of the rotation center to structural discontinuities (e.g., a band of connective tissue or coronary vessels). Theoretically, the larger the κ_c, the stronger the interaction between the SW tip and the unexcitable obstacles (26). A decrease of κ_c by bepridil would, therefore, prevent anchoring.

As described so far, destabilization of SW reentry in the presence of bepridil facilitated self-termination as a result of prominent drift of the rotation center followed by collision with anatomical boundaries. However, excessive SW destabilization in association with marked APD prolongation would promote SW breakup, leading to degeneration of tachycardia to multiple wavelet-type fibrillation. Bepridil-induced TdP and VF have been reported to be more prevalent in patients with structural heart diseases, hypokalemia or bradycardia, conditions known to reduce the ventricular repolarization reserve (1, 40).

In summary, the bepridil-induced destabilization and early termination of SW reentry, which is not associated with an increase of wavebreaks, may be attributable to a combination of moderate APD prolongation and inhibition of wave propagation with high convex curvature resulting from an enhancement of intercellular electrical coupling.

Limitations

There are several limitations in this study. First, we investigated the electrophysiological mechanisms for the antiarrhythmic effects of bepridil using 2-dimensional ventricular myocardium to facilitate the analysis of SW dynamics. Care should be taken in extending the results to 3-dimensional hearts in larger animals including humans. When there is sufficient tissue mass, the chance of spontaneous termination of rotors by collision with anatomical boundaries would be reduced, whereas the enhancement of rotor drift and SW instability might promote transition from VT to VF. Physiological transmural

twist of myofiber orientation and structural discontinuities and functional heterogeneities in diseased hearts would also alter the requirements for termination of reentry. Second, we used BDM as an excitation-contraction uncoupler, which alters ionic currents and intracellular Ca^{2+} dynamics. However, this does not seem to invalidate the present results because the characteristic modification of SW dynamics by bepridil was preserved in the absence of BDM (Supplementary Fig. 2: available in the online version only). Despite these limitations, the present study provides a new perspective on the mechanism for the unique and potent antiarrhythmic action of bepridil.

Conclusions

Bepridil at a therapeutic concentration (1 μM) causes a moderate prolongation of APD and an increase of intercellular electrical coupling of cardiac muscle. This combination compromises wavefront propagation in the rotation center of SW reentry, leading to drift and early termination.

Acknowledgments

Bepridil was kindly supplied from Dai-ichi Sankyo Corporation (Tokyo). The authors thank Dr. Satoko Ito and Dr. Toshinori Hyodo, Division of Cancer Biology, Nagoya University for the technical support of dye-transfer experiments. This study was financially supported by a Grant-in-Aid for Scientific Research (B) 19390210 and a Grant-in-Aid for Scientific Research (C) 20590860 from the Japanese Society for Promotion of Sciences and a Grant-in-Aid for Scientific Research on Innovative Area 22136010 from the Ministry of Education, Culture, Sports, Science, and Technology, Japan.

References

1 Gill A, Flaim SF, Damiano BP, Sit SP, Brannan MD. Pharmacology of bepridil. Am J Cardiol. 1992;69:11–16.
2 Sugao M, Fujiki A, Nishida K, Sakabe M, Tsuneda T, Iwamoto J, et al. Repolarization dynamics in patients with idiopathic ventricular fibrillation: Pharmacological therapy with bepridil and disopyramide. J Cardiovasc Pharmacol. 2005;45:545–549.
3 Izumi D, Chinushi M, Watanabe H, Washizuka T, Okumura K, Komura S, et al. Bepridil for drug-refractory ventricular tachyarrhythmias. Intern Med. 2007;46:119–124.
4 Fujiki A, Tsuneda T, Sugao M, Mizumaki K, Inoue H. Usefulness and safety of bepridil in converting persistent atrial fibrillation to sinus rhythm. Am J Cardiol. 2003;92:472–475.
5 Yamashita T, Ogawa S, Sato T, Aizawa Y, Atarashi H, Fujiki A, et al. Dose-response effects of bepridil in patients with persistent atrial fibrillation monitored with transtelephonic electrocardiograms: A multicenter, randomized, placebo-controlled, double-blind study (J-BAF study). Circ J. 2009;73:1020–1027.
6 Sato N, Nishimura M, Kawamura Y, Ward CA, Kikuchi K. Blocks of Na^+ channel by bepridil in isolated guinea-pig ventricular myocytes. Eur J Pharmacol. 1996;314:373–379.
7 Yatani A, Brown AM, Schwartz A. Bepridil block of cardiac calcium and sodium channels. J Pharmcol Exp Ther. 1986;237:9–17.
8 Uchino T, Lee TS, Kaku T, Yamashita N, Noguchi T, Ono K. Voltage-dependent and frequency-independent inhibition of recombinant $Ca_v3.2$ T-type Ca^{2+} channel by bepridil. Pharmacology. 2005;74:174–181.
9 Watanabe Y, Kimura J. Blocking effect of bepridil on Na^+/Ca^{2+} exchange current in guinea pig cardiac ventricular myocytes. Jpn J Pharmacol. 2001;85:370–375.
10 Wang JC, Kiyosue T, Kiriyama K, Arita M. Bepridil differentially inhibits two delayed rectifier K^+ currents, I_{Kr} and I_{Ks}, in guinea-pig ventricular myocytes. Br J Pharmacol. 1999;128:1733–1738.
11 Kobayashi S, Reien Y, Ogura T, Saito T, Masuda Y, Nakaya H. Inhibitory effect of bepridil on $hK_v1.5$ channel current: comparison with amiodarone and E-4031. Eur J Pharmacol. 2001;430:149–157.
12 Berger F, Borchard U, Hafner D. Effects of the calcium entry blocker bepridil on repolarizing and pacemaker currents in sheep cardiac Purkinje fibers. Naunyn Schmidebergs Arch Pharmacol. 1989;339:638–646.
13 Li Y, Sato T, Arita M. Bepridil blunts the shortening of action potential duration caused by metabolic inhibition via blockade of ATP-sensitive K^+ channels and Na^+-activated K^+ channels. J Pharmacol Exp Ther. 1999;291:562–568.
14 Hara Y, Nakaya H. SD-3212, a new class I and IV antiarrhythmic drug: a potent inhibitor of the muscarinic acetylcholine-receptor-operated potassium current in guinea-pig atrial cells. Br J Pharmacol. 1995;116:2750–2756.
15 Sato T, Costa AD, Saito T, Ogura T, Ishida H, Garlid KD, et al. Bepridil, an antiarrhythmic drug, opens mitochondrial K_{ATP} channels, blocks sarcolemmal K_{ATP} channels, and confers cardioprotection. J Pharmacol Exp Ther. 2006;316:182–188.
16 Itoh H, Ishikawa T, Hidaka H. Effects on calmodulin of bepridil, an antianginal agent. J Pharmacol Exp Ther. 1984;230:737–741.
17 Li Y, Love ML, Putkey JA, Cohen C. Bepridil opens the regulatory N-terminal lobe of cardiac troponin C. Proc Natl Acad Sci U S A. 2000;97:5140–5145.
18 Jalife J. Ventricular fibrillation: mechanisms of initiation and maintenance. Annu Rev Physiol. 2000;62:25–50.
19 Weiss JN, Qu Z, Chen PS, Lin SF, Karagueuzian HS, Hayashi H, et al. The dynamics of cardiac fibrillation. Circulation. 2005;112:1232–1240.
20 Yamazaki M, Honjo H, Nakagawa H, Ishiguro YS, Okuno Y, Amino M, et al. Mechanisms of destabilization and early termination of spiral wave reentry in the ventricle by a class III antiarrhythmic agent, nifekalant. Am J Physiol Heart Circ Physiol. 2007;292:H539–H548.
21 Harada M, Honjo H, Yamazaki M, Nakagawa H, Ishiguro YS, Okuno Y, et al. Moderate hypothermia increases the chance of spiral wave collision in favor of self-termination of ventricular tachycardia/fibrillation. Am J Physiol Heart Circ Physiol. 2008;294:H1896–H905.
22 Ishiguro YS, Honjo H, Opthof T, Okuno Y, Nakagawa H, Yamazaki M, et al. Early termination of spiral wave reentry by combined blockade of Na^+ and L-type Ca^{2+} currents in a perfused two-dimensional epicardial layer of rabbit ventricular myocardium. Heart Rhythm. 2009;6:684–692.
23 Gray RA, Pertsov AM, Jalife J. Spatial and temporal organization during cardiac fibrillation. Nature. 1998;392:75–78.

24 Akar FG, Roth BJ, Rosenbaum DS. Optical measurement of cell-to-cell coupling in intact heart using subthreshold electrical stimulation. Am J Physiol Heart Circ Physiol. 2001;281:H533–H542.
25 Sato T, Ohkusa T, Honjo H, Suzuki S, Yoshida MA, Ishiguro YS, et al. Altered expression of connexin43 contributes to the arrhythmogenic substrate during the development of heart failure in cardiomyopathic hamster. Am J Physiol Heart Circ Physiol. 2008;294:H1164–H1173.
26 Kléber AG, Rudy Y. Basic mechanisms of cardiac impulse propagation and associated arrhythmias. Physiol Rev. 2004;84:431–488.
27 Cabo C, Pertsov AM, Baxter WT, Davidenko JM, Gray RA, Jalife J. Wave-front curvature as a cause of slow conduction and block in isolated cardiac muscle. Circ Res. 1994;75:1014–1028.
28 Bayly PV, KenKnight BH, Rogers JM, Hillsley RE, Ideker RE, Smith WM. Estimation of conduction velocity vector fields from epicardial mapping data. IEEE Trans Biomed Eng. 1998;45:563–571.
29 Nakagami T, Tanaka H, Dai P, Lin SF, Tanabe T, Mani H, et al. Generation of reentrant arrhythmias by dominant-negative inhibition of connexin43 in rat cultured myocyte monolayers. Cardiovasc Res. 2008;79:70–79.
30 Osaka T, Kodama I, Toyama J, Yamada K. Effects of bepridil on ventricular depolarization and repolarization of rabbit isolated hearts with particular reference to its possible proarrhythmic properties. Br J Phrmacol. 1988;93:775–780.
31 Nobe S, Aomine M, Arita M. Bepridil prolongs the action potential duration of guinea pig ventricular muscle only at rapid rates of stimulation. Gen Pharmacol. 1993;24:1187–1196.
32 Kato R, Singh BN. Effects of bepridil on the electrophysiologic properties of isolated canine and rabbit myocardial fibers. Am Heart J. 1996;111:271–279.
33 Osaka T, Yokoyama E, Kushiyama Y, Hasebe H, Kuroda Y, Suzuki T, et al. Opposing effects of bepridil on ventricular repolarization in humans: inhomogeneous prolongation of the action potential duration vs flattening of its restitution kinetics. Circ J. 2009;73:1612–1618.
34 Winfree AT. Heart muscle as a reaction-diffusion medium: the roles of electric potential diffusion, activation front curvature, and anisotropy. Int J Bifurc Chaos. 1997;7:487–526.
35 Cabo C, Pertsov AM, Davidenko JM, Jalife J. Electrical turbulence as a result of the critical curvature for propagation in cardiac tissue. Chaos. 1998;8:116–126.
36 Knisely SB, Hill BC. Effects of bipolar point and line stimulation in anisotropic rabbit epicardium: assessment of the critical radius of curvature for longitudinal lock. IEEE Trans Biomed Eng. 1995;42:957–966.
37 Peracchia C. Chemical gating of gap junction channels; roles of calcium, pH and calmodulin. Biochim Biophys Acta. 2004;1662:61–80.
38 Toyama J, Sugiura H, Kamiya K, Kodama I, Terasawa M, Hidaka H. Ca^{2+}-calmodulin mediated modulation of the electrical coupling of ventricular myocytes isolated from guinea pig heart. J Mol Cell Cardiol. 1994;26:1007–1015.
39 Zhou Y, Yang W, Lurtz MM, Ye Y, Huang Y, Lee HW, et al. Identification of the calmodulin binding domain of connexin 43. J Biol Chem. 2007;282:35005–35017.
40 Singh BN. Safety profile of bepridil determined from clinical trials in chronic stable angina in the United States. Am J Cardiol. 1992;69:68D–74D.